Electronic Supplementary Information (ESI)

Rituxan Nano-Conjugation Prolongs Drug/Cell Interaction and Enables Simultaneous Depletion and Enhanced Raman Detection of Lymphoma Cells

Qian Yao [a], Fei Cao [a], Marion Lang [a], Chao Feng[b], Xiaotong Meng [a], Yongzhe Zhang, [c] Yan Zhao[b] and Xiu-hong Wang [a] *

ESI includes:

1. Quantification of Rituxan and calculation of loading capacity; *In vitro* release of Rituxan; ADCC (Antibody-Dependent Cell-mediated Cytotoxicity); Working principle of the Imaging Flow Cytometry (IFC);

2. Supplementary Figures (Fig. S1-S8): Characterization of the nanoparticles based on 10-nm and 50-nm AgNPs, Rituxan release from nanoconjugates in PBS(pH=7 .4), Dose-response curves of the ADCC assay, LSCM results of CD20 negative SK-BR3 cells treated with 50-nm Rituxan nanoconjugates and free Rituxan, Cells viability after the treatment with Ag-pMBA or Rituxian nanoconjugates, Apoptotic results of Raji or Daudi cells treated with Rituxan and Rituxan nanoconjugates; SERS spectra of 50-nm Ag-pMBA and Rituxan nanoconjugates;

3. Supplementary References.

1.

Quantification of Rituxan and calculation of loading capacity. Bovine Serum Albumin (BSA) was used to plot the standard curve for the assay. Doses of 0, 1, 2, 4, 8, 12, 16 and 20 μL BSA (100μg/ml) were added to eight wells of a 96-well plate, respectively. Then wells were filled with 20uL PBS. 20μL samples were added to other wells. Then, 200μl of G-250 dye was added to each well and mixed well. The mixtures were incubated at room temperature (RT) for 3-5 min. The absorbance at 595 nm of each well was measured using a microplate reader. The protein concentrations were calculated using the standard curve. The quantities of unconjugated and conjugated Rituxan were measured in parallel to avoid experimental errors.
The quantity of AgNPs was determined by measuring the plasmonic absorption at 431 nm for 50-nm Rituxan nanoconjugates, and the loading capacity was calculated.[1, 2] To compare with the predicted loading, the theoretical calculation of the loading capacity was performed as follows [Eq. (1-3)]:

$$\text{Predicted adsorption foot print, or PAF } (m^2/mg)=(A*N_A)/(1000*\theta_m) \quad (1)$$

$$\text{Surface area of a sphere: } S=4\pi R^2 \quad (2)$$

$$\text{Loading ratio}=(S*N_A)/(PAF*M) \quad (3)$$

Here, A is the projected area of the adsorbed mAb molecule on the surface (m^2), N_A is the Avogadro's number (molecules/mole), M is the molecular weight of the Rituxan (g/mol), and θ_m is the assumed packing efficiency. For the projection of a disc of equivalent diameter (D) to the mAb on the surface, the adsorbed area is given by: $A=\pi D^2/4$ .We calculated the footprint and loading for close packing (θ_m=1) on the surface, D=6.92 nm, M=144kDa, R=25nm.

***In vitro* release of Rituxan.** *In vitro* release of Rituxan from the 50-nm Rituxan nanoconjugates was performed in PBS (pH 7.4). The nanoconjugates were resuspended in 1 mL PBS (concentration of Rituxan is 40μg/mL) and incubated at 37°C. At scheduled time intervals (1h, 2h, 4h, 8h, 18h and 24h) sample was centrifugated (14,000 rpm, 10 minutes) and the whole supernatant was replaced with fresh PBS. Then, the Rituxan content in the supernatants was measured with BCA assay.

ADCC (Antibody-Dependent Cell-mediated Cytotoxicity). To evaluate the binding of Rituxan nanoconjugates to the lymphoma cells and mediating the antibody-dependent cell-mediated cytotoxicity (ADCC) effect for Daudi cells, NK92 cells were isolated from human peripheral blood mononuclear cells (PBMCs). The Daudi cells and NK92 cells were used as target cells and effector cells, respectively. The target cells were collected by centrifuging the solution at 800 rpm for 3 minutes and washed with assay buffer. After being seeded onto 96-well plates (2×10^5 cells/mL, 50μL/well), Daudi cells were incubated for 30 min in the medium containing 10-nm nanoconjugates at varying antibody concentrations (0.00001, 0.0001, 0.001, 0.01, 0.1, 1, and 10μg/mL, 50μL/well) in a humidified incubator at 37°C, 5% CO_2. Then, NK92/ FcRγ3a cells (1×10^5 cells/mL) were added into corresponding wells (50μL/well) following gentle vortex-mixing and incubation for 6 h at 37°C, 5% CO_2. After centrifugation at 1,000 rpm, 50μL of the supernatant

was collected and applied into new 96-well plates. Finally, 50μL LDH detection liquid was added to each well and incubated for 30 min at RT. The absorbance was measured at 492nm with FlexStation3 (Molecular Devices), using 650nm as the background wavelength. The Rituxan nanoconjugates were diluted with MEM medium without phenol red (containing 1% FBS and 1% of green/streptomycin). Cells incubated with Rituxan and Herceptin were used as control. The pyrolysis percentage of cells caused by ADCC effect was calculated using [Eq. (4)]:

$$\text{Cell lysis} = (OD_{\text{experimental data}} - OD_{\text{background}}) / (OD_{\text{Maximum release}} - OD_{\text{Minimum release}}) \times 100\% \quad (4)$$

Working principle of the Imaging Flow Cytometry (IFC). The FlowSight imaging flow cytometry (IFC) was developed to integrate Flow Cytometry and Microscopy in a single instrument platform for cell analysis. It utilizes an optical system, the extended depth of field (EDF™), which allows to image structures in cells with a depth of field (a couple of micrometers). The fluorescence images taken by the machine were not a projection of the whole cell, but show a cross-sectional image with a depth of focus.[3] The fluorescence images are then overlaid with the brightfield images. The image processing algorithm then can determine the internalization factor.

Cellular processes such as drug uptake and processing by cells, entry of nanoparticles and toxins, can be studied on FlowSight imaging flow cytometers by measuring internalization features. The system automatically collects large numbers of images per data set and provides quantitative image analysis tools that facilitate the objective and rapid localization of internalized probes. Following the statistical analysis of the large number of images by IDEAS software, internalization features can be plotted. Cells that show internalization typically have positive scores while cells with little internalization have negative scores. Cells with scores around 0 have a mix of internalization and membrane intensity.

2. Supplementary Figures

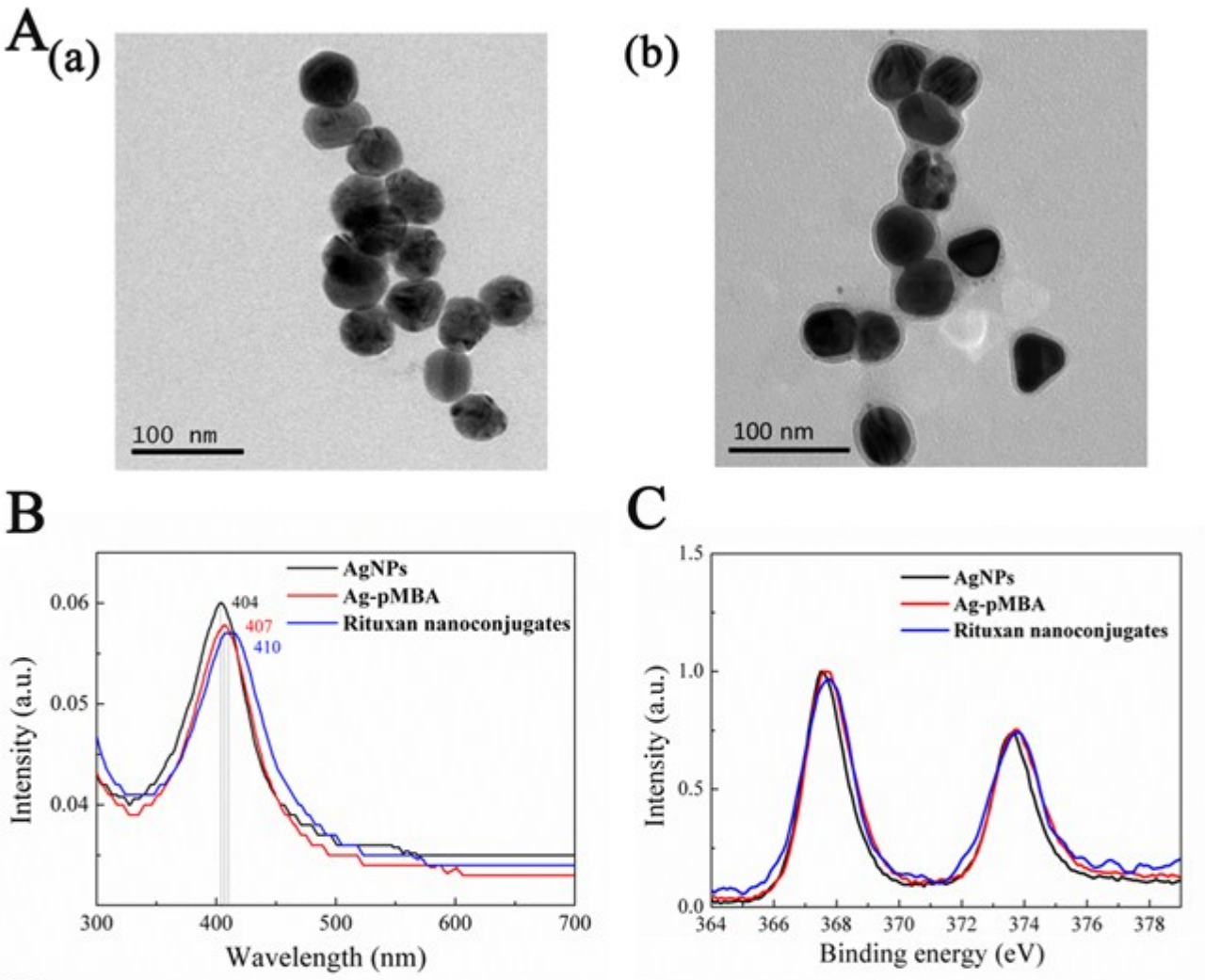

D

Samples		Zeta potential values (mV)
10-nm	AgNPs	-26.9±6.82
	Ag-pMBA	-18.4±6.86
	Rituxan nanoconjugates	-10.2±4.31
50-nm	AgNPs	-37.3±18.1
	Ag-pMBA	-30.3±10.8
	Rituxan nanoconjugates	-9.79±8.49

Fig. S1 (A) Morphologic analysis by transmission electron microscopy (TEM) of (a) uncoated AgNPs and (b) Rituxan Nanoconjugates based on 50-nm silver nanoparticles. (B) The extinction spectra and (C) High-resolution Ag3d X-ray photoelectron spectra obtained from 50-nm AgNPs, Ag-pMBA and Rituxan Nanoconjugates. (D) Zeta potential values of 10-nm AgNPs, Ag-pMBA and Rituxan Nanoconjugates.

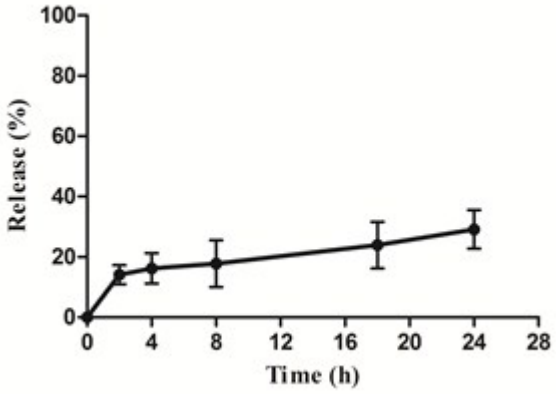

Fig. S2 Rituxan release from nanoconjugates in PBS (pH=7 .4).

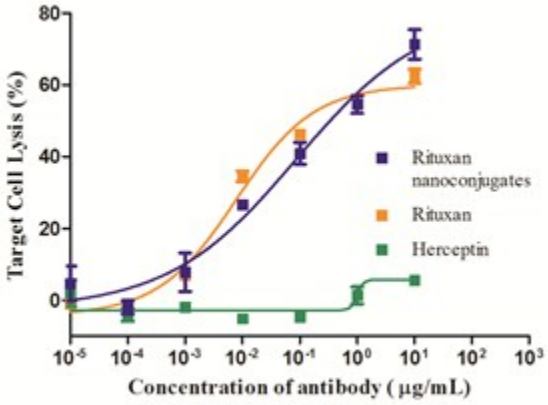

Fig. S3 Dose-response curves of the ADCC assay.

As shown in Fig.S3, in the concentration range from 0.00001 to 10μg/mL, conjugated Rituxan induced a dose-dependent lysis of Daudi cells, with similar potency to free Rituxan molecules (Figure 3b). The non-specific antibody Herceptin did not cause any cell lysis. The maximum percentage of lysed Daudi cells was ~60% for free Rituxan, whereas at a concentration of 10μg/mL, Rituxan nanoconjugates lysed 75% of the Daudi cells. Rituxan nanoconjugates could potentially kill more cells if the concentration was increased. The results clearly indicate that the synthesized nanoconjugates retained the ability of Rituxan to bind CD20 molecules and mediate ADCC.

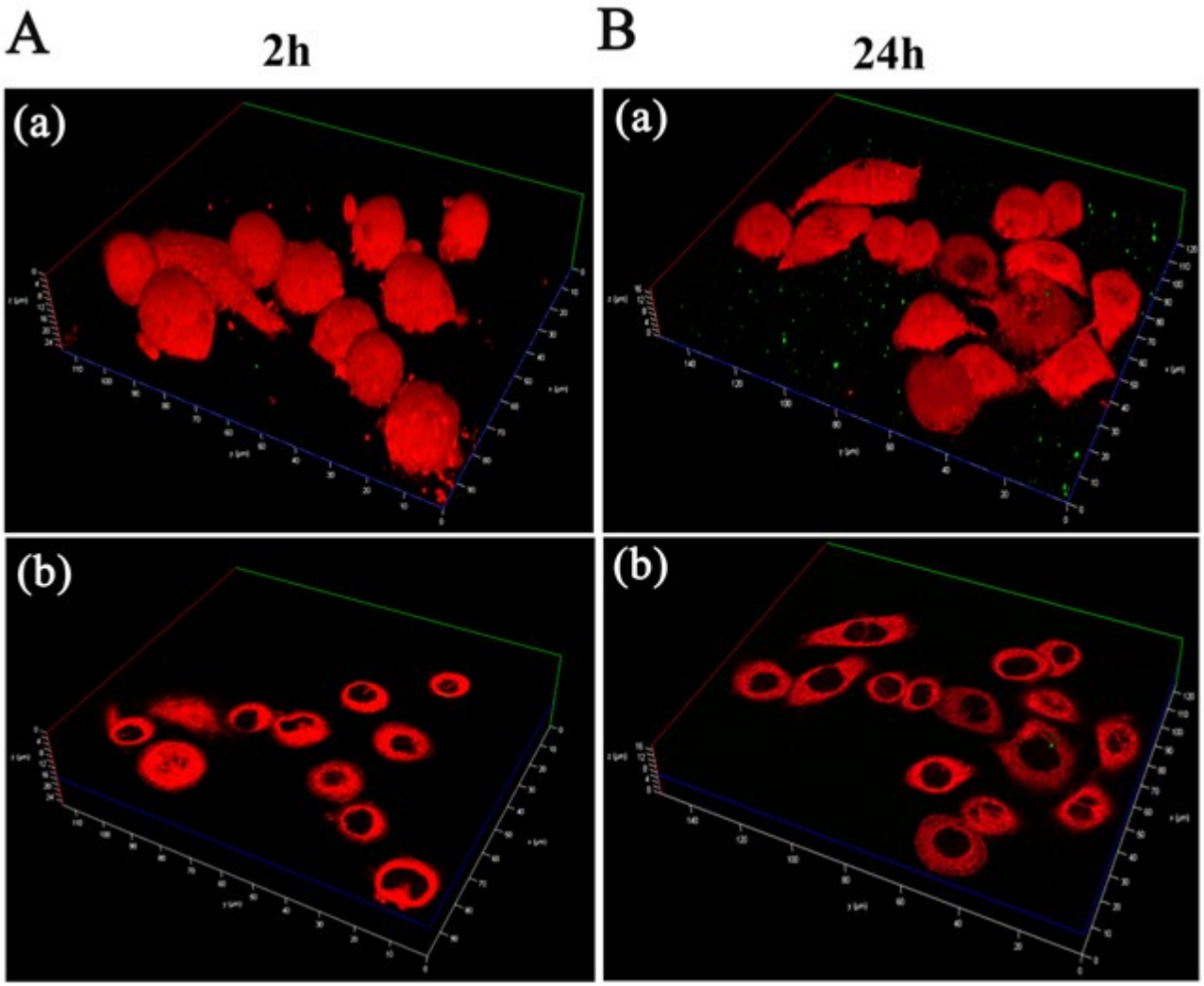

Fig. S4 CD20(-) SK-BR3 cells were treated with 50-nm Rituxan nanoconjugates for (A) 2h and (B) 24h. Images show (Aa, Ba) 3D renderingsand and (Ab, Bb) cross sections of the LSCM images after 2h and 24h, respectively. Red: cells labeled with CellMask™ Deep Red. Green: free-Rituxan and nanoconjugate labeled with AF 488 fluorescent dye *via* Rituxan molecules.

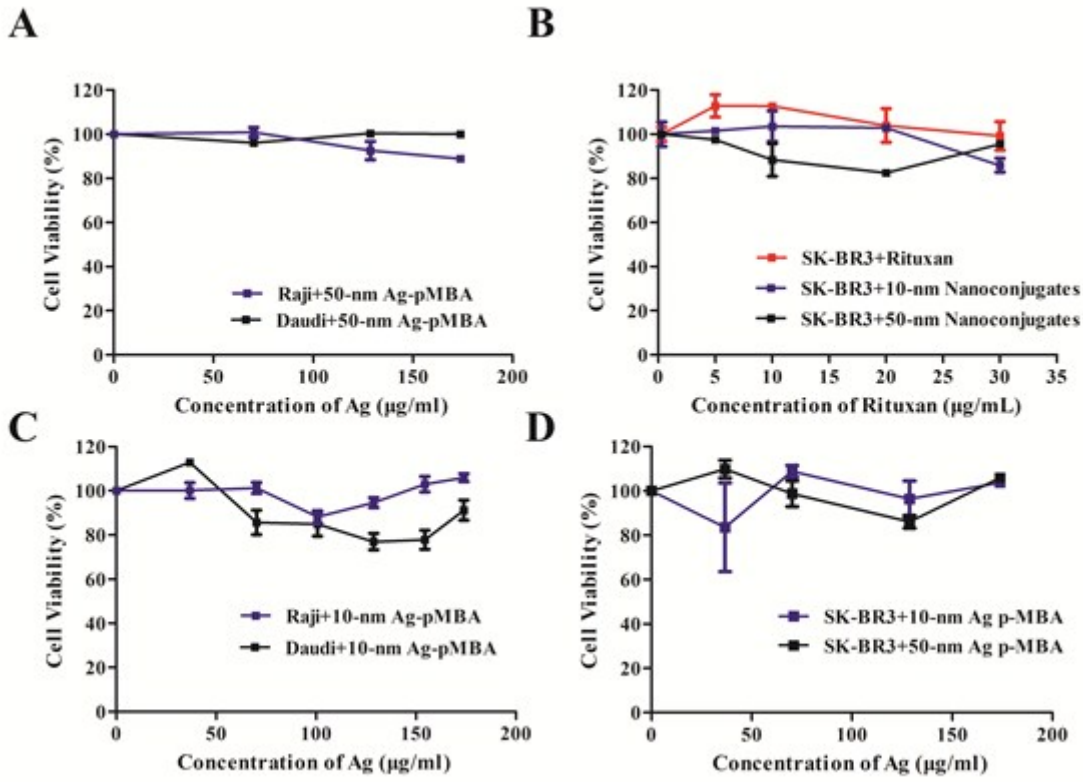

Fig. S5 (A) p-MBA-coated AgNPs show no toxic effect on lymphoma cell lines Raji (blue) and Daudi (black). (B) Free Rituxan and Rituxan nanoconjugates are not toxic to CD20(-) breast cancer cells SK-BR3. (C) Cell viability of Raji (blue) and Daudi cells (black) after being treated with varying concentrations of 10-nm Ag-pMBA. (D) p-MBA coated 10-nm AgNPs (blue) and 50-nm AgNPs (black) are not toxic to breast cancer cells SK-BR3.

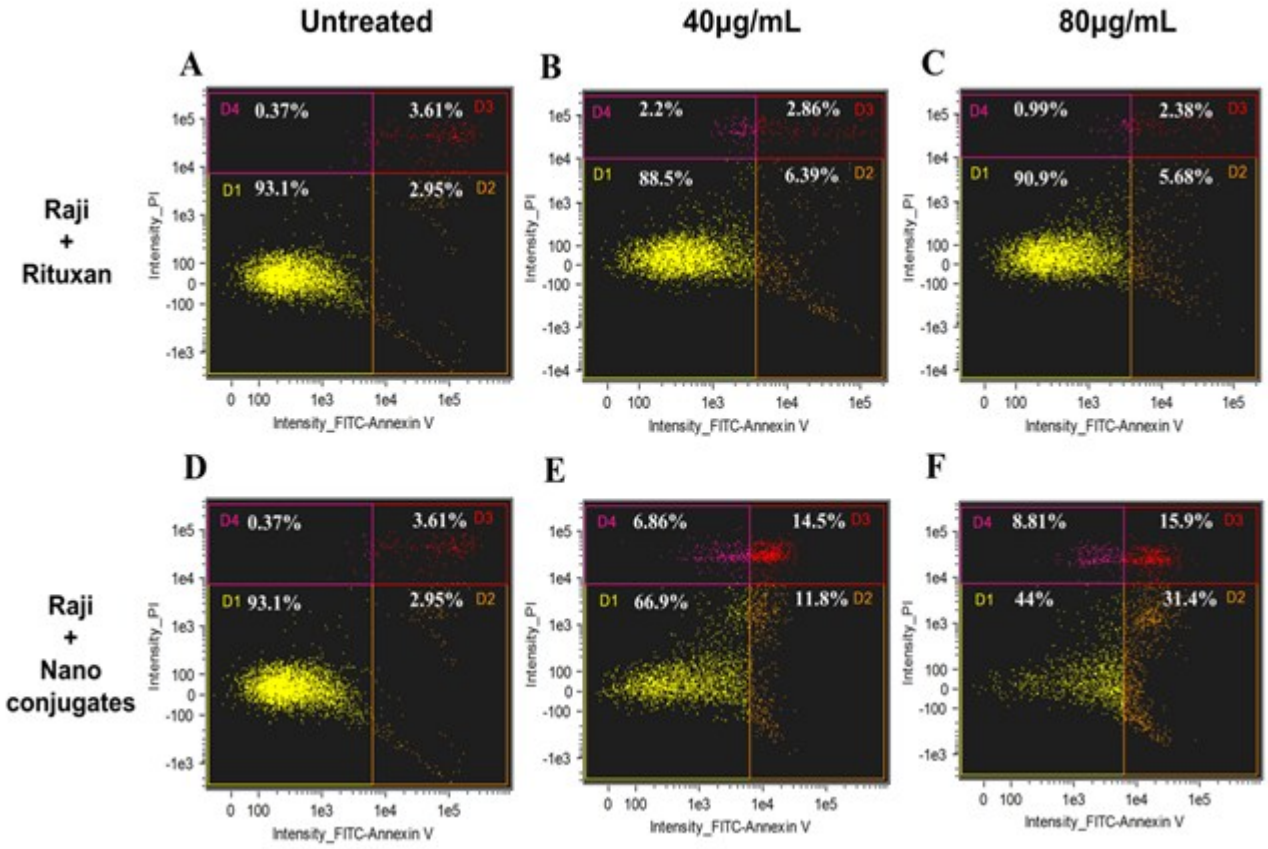

Fig. S6 Dot plots of apoptotic Raji cells stained with Annexin V-FITC/PI. (A-C) Free Rituxan and (D-F) Rituxan nanoconjugates treatment at concentrations of 0,40 and 80μg/mL (Rituxan concentration) for 12h. D1: living cells, D2: early apoptosis, D3: late apoptosis, D4: necrosis.

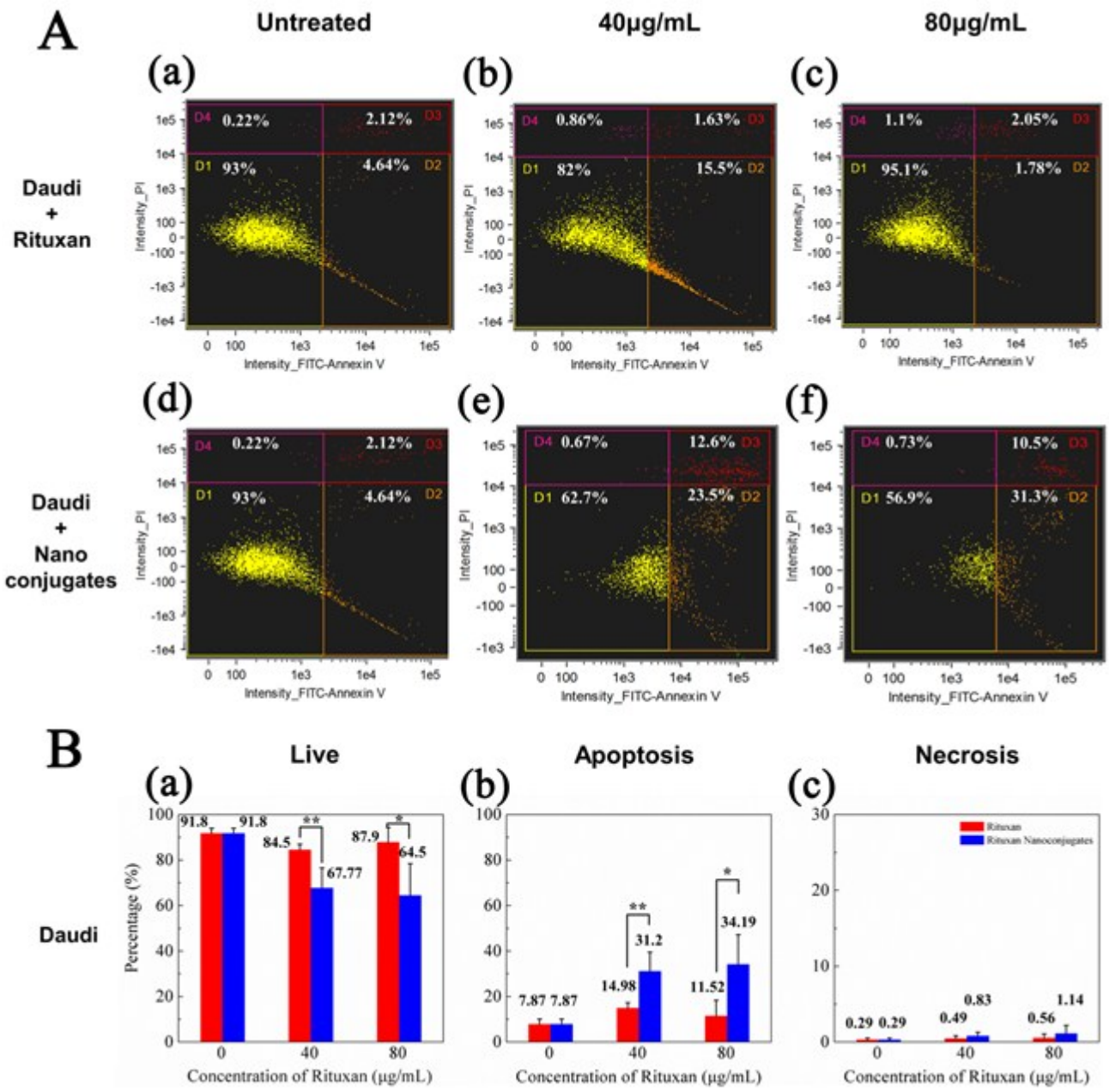

Fig. S7 Synthesized nanoconjugates enhanced apoptosis of lymphoma cells. (A) Apoptotic results by Annexin V/PI staining of Daudi cells treated with Rituxan (a-c) and 10-nm Rituxan Nanoconjugates (d-f) (0, 40, 80μg/mL) for 12h. D1: living cells, D2: early apoptosis, D3: late apoptosis, D4: necrosis. (B) Induction of Daudi cells' status after treatment with Rituxan and 10-nm Rituxan Nanoconjugates, respectively treatment as shown in a. Data are mean of three individual experiments. 0.05<p<0.1*,0.01<p<0.05 **, p<0.01***.

Fig. S6 and Fig. S7a show the dot-plots of apoptotic cells. Cells in the lower-right (Annexin V-FITC positive, PI negative) and up-right regions (both Annexin V-FITC and PI positive) represent early and late apoptotic cells, respectively; cells in the lower-left (unstained) and up-left regions (only PI positive) represent live and necrotic (or dead) cells, respectively.

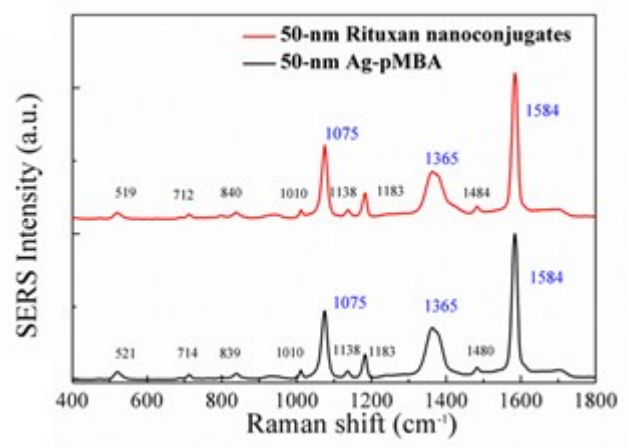

Fig. S8 SERS spectra acquired from 50-nm p-MBA-coated AgNPs (black) and Rituxan nanoconjugates (red).

Supplementary References

1 J. S. Bee, D. Chiu, S. Sawicki, J. L. Stevenson, K. Chatterjee, E. Freund, J. F. Carpenter and T. W. Randolph, *J. Pharm. Sci.* 2009, **98**, 3218−3238.

2 H. P. Erickson, *Biol. Proced. Online* 2009, **11**, 32-51.

3 Y. Yan, A. P. R. Johnston, S. J. Dodds, M. M. J. Kamphuis, C. Ferguson, R. G. Parton, E. C. Nice, J. K. Heath and F. Caruso, *ACS Nano* 2010, **4**, 2928-2936.